THE AMERICAN SOCIETY OF MECHANICAL ENGINEERS
345 E. 47th St., New York, N.Y. 10017

97-GT-455

AN EXPERIMENTAL INVESTIGATION OF TRANSITION AS APPLIED TO LOW PRESSURE TURBINE SUCTION SURFACE FLOWS

Songgang Qiu and Terrence W. Simon
Heat Transfer Laboratory
Department of Mechanical Engineering
University of Minnesota
Minneapolis, Minnesota

ABSTRACT

Results are presented of an experimental study of separation and transition within the flow over the suction surface of a low-pressure turbine airfoil. Detailed velocity profiles, measured in the near-wall region with the hot-wire technique, and surface static pressure distributions are presented. Flow transition is documented using measured intermittency distributions in the attached boundary layer and within the separated shear layer. Cases for Reynolds numbers based on exit velocity and suction surface length of 50,000, 100,000, 200,000, and 300,000 under low Free Stream Turbulence Intensity (FSTI=0.5%), moderate-FSTI (2.5%), and high-FSTI (10%) are reported. Cases of FSTI=2.5%, which, due to wakes, are most representative of low-pressure turbine flows, are discussed in detail. Comparisons are made for cases of differing Reynolds numbers and FSTI values. Flow separation, with transition of the shear layer over the separation bubble, is observed for the lower-Re cases. Enhanced transport after flow transition reduces the separation bubble size and eventually accelerates the near-wall flow to attached boundary layer status. Elevated FSTI and increased Re promote earlier transition, smaller separation bubbles, and an increased possibility that the boundary layer will remain attached and transition as such. Models for intermittency distribution, transition onset location, and transition length are assessed.

NOMENCLATURE

$C_p=2(p_t-p)/\rho U_e^2$	static pressure coefficient
FSTI	turbulence level in the approach flow
L=11.43 cm	true chord length
L_x=10.16 cm	axial chord length
L_{ss}=15.49 cm	suction surface length
p	static pressure (Pa)
p_t	total pressure (Pa)
$Re=L_{ss}U_e/\nu$	Reynolds number
s	distance along the suction surface (m)
$TI=u'_{rms}/u$	turbulence intensity
$TIe = FSTI\frac{U_{in}}{U_\infty}$	local turbulence intensity used in Eqn. 4
u'_{rms}	local rms fluctuation of velocity (m/sec)
u	ensemble-averaged local velocity (m/sec)
U_e	exit velocity (m/sec)
U_{in}	velocity of approach flow (m/sec)
U_∞	free-stream velocity (m/sec)
x	axial position (m)
y	distance normal to the wall (m)
δ	boundary layer thickness (m)
δ_2	momentum thickness (m)
γ	intermittency
ν	kinematic viscosity (m^2/sec)

INTRODUCTION

In recent years, new demands for improved performance have driven the gas turbine industry to search for innovative techniques for improved aerodynamic performance. In support of these objectives, efforts have been made to strengthen the understanding of transport processes within the very complex flow of gas turbines. One concern is the lack of understanding about boundary layer transition and separation within an environment which is representative of turbomachine airfoil passages. The state of a transitional boundary layer is often described in terms of intermittency (the fraction of the flow that is turbulent-like or the fraction of the time the flow is turbulent-like), and the state of a turbulent boundary layer is characterized in terms of its maturity, usually given as the momentum thickness Reynolds number. The description of the flow is particularly difficult on the suction side of low-

Presented at the International Gas Turbine & Aeroengine Congress & Exhibition
Orlando, Florida — June 2–June 5, 1997

pressure turbine airfoils, where separation bubbles are believed to cause a significant degradation of engine efficiency (Sharma et al., 1994), particularly at altitude and during off-design operation. The location and extent of these separation regions depend on the history of streamwise development of the boundary layer and the nature of the flow external to the separation bubble. Thus, the full history of the boundary layer development must be known and the boundary layer's response to all destabilizing influences must be assessed.

Mayle (1991), in a review of laminar-to-turbulent transition and its impact on gas turbine engine design, stated that a substantial fraction of the boundary layer on each side of a gas turbine airfoil may be transitional. He described various transition modes and their roles in gas turbine engines. Various correlation equations were then developed and suggested for each of the transition modes. In this paper, some of his models for transition length and location are assessed by comparison with experimental data.

In the flow passage under study, strong acceleration on the upstream portion of the blade prevents flow transition and deceleration downstream of the throat of the passage promotes flow separation. If the flow separates, the shear layer over the separation bubble becomes unstable and transitions. The enhanced transport due to turbulence will reduce the bubble size and may eventually eliminate the separated flow region. With elevated disturbance levels in the approach flow (the present study), the boundary layer will transition without separation in some cases and will separate, then transition, in others.

Halstead et al. (1995) conducted an experimental study of boundary layer flows on airfoil surfaces in compressors and low-pressure turbines which closely simulated actual gas turbine engine components. In their tests, surface measurements were made with surface-mounted, hot-film gauges and free-stream velocities between airfoil rows were measured with hot-wire probes. Their experiments showed large regions of laminar and transitional flow on the suction surface, with the boundary layer generally developing along two distinct, but coupled, paths -- under the wakes of upstream airfoils and between wakes. In their simulation of low-pressure turbines, FSTI under the wakes was 2.5-3% and between the wakes was around 1.5%. They found that calmed regions followed the turbulent spots which were produced in the wake paths. These calmed regions were effective in suppressing flow separation and delaying transition. They observed bypass transition and separated-flow transition on both suction and pressure surfaces. Recent work of Malkiel and Mayle (1995) of laminar shear layer transition over separation bubbles suggested that intermittency in separation bubbles can be modeled with correlations developed for attached boundary layer flows and that Kelvin-Helmhotz vortex pairing exists in this transition region, similar to that observed in free shear layers.

At higher FSTI (8.6%) and on a 97 cm-radius, concave curved, unaccelerated flow, Kim et al. (1994), showed that transition occurred near the leading edge of the test wall and the flow was fully turbulent downstream. Effects of mild ($K=0.75\times10^{-6}$) acceleration rates on a 97 cm-radius, concave curved boundary layer flow, reported by Volino and Simon (1994, 1995a), noted that transition was little influenced by acceleration. In a stronger-acceleration case ($K=10\times10^{-6}$, Volino and Simon, 1995b, 1995c) acceleration significantly lengthened the transition zone. Also, at the beginning of the test section, where the acceleration effect was strongest, there was some evidence of a reverse transition (from turbulent to laminar flow). This happened in spite of the high (~8%) inlet free-stream turbulence level. Two different regions of the transitional boundary layer were identified. The first was a severely disturbed, non-turbulent flow characterized by high-amplitude unsteadiness, with energy distributed over a range of relatively low frequencies. Within this non-turbulent region, little turbulent transport was found and the role of the wall (and, hence, the boundary layer) was to dampen the amplitude and reduce the scales from those of the free-stream turbulence. Downstream was a region of turbulent flow, possessing high-amplitude fluctuations and having energy distributed over a wide range of scales.

Mayle (1991) suggested the following correlations for the length from separation to transition and the length of transition in terms of momentum thickness Reynolds number at separation,

$$Re_{s_{st}} = 300\, Re_{\delta 2_s}{}^{0.7} \quad \text{(short bubble)} \tag{1}$$

$$Re_{s_{st}} = 1000\, Re_{\delta 2_s}{}^{0.7} \quad \text{(long bubble), and} \tag{2}$$

$$Re_{LT} = 400\, Re_{\delta 2_s}{}^{0.7} \tag{3}$$

where $Re_{s_{st}}$ is the Reynolds number based on distance from separation to transition and Re_{LT} is the Reynolds number based on transition length. Roberts (1973, 1980) developed a correlation for the length from separation to transition in terms of both the turbulence level and turbulence length scale. Davis et al. (1985) modified it yielding the correlation :

$$Re_{s_{st}} = 25{,}000 \log_{10}(\coth[17.32 TIe]) \tag{4}$$

where TIe is the local turbulence intensity, given as

$$TIe = FSTI \frac{U_{in}}{U_{\infty}}.$$

In this paper, results are presented from a flow that simulates the suction surface flow of a low-pressure gas turbine airfoil, including the combined effects of Reynolds number, free stream turbulence, curvature, and acceleration. This paper addresses the stated need to improve performance of low-pressure turbine stages and to improve the understanding of flow transition and separation on the suction surface of a modern, low-pressure turbine airfoil under various free-stream disturbance levels and with representative curvature and acceleration profiles. Compressibility, rotation, and passing wake effects are not considered in this study.

FACILITY AND INSTRUMENTATION

All experiments were performed in a low-speed, open-return, blown-type wind tunnel. The wind tunnel exit is connected to a rectangular settling duct which matches the tunnel's nozzle exit dimensions, followed by a test section (cascade simulator). A general layout of the test section is given in Fig. 1. Three different turbulence levels, 0.5%, 2.5%, and 10%, were achieved. No active turbulence generation was employed in the 0.5% FSTI case. Elevated disturbance levels were produced by installing turbulence generators in the settling duct, a passive rod-grid between the nozzle exit and the transition duct inlet to achieve 2.5% and a passive bar-grid at that location and a jet grid 45.5 cm downstream to achieve 10%. The airfoil leading edge is 66.5 cm downstream of the jet grid. The technique for generating high turbulence was a modification of the one which Sahm and Moffat (1992)

developed. For recording channel static pressures, three columns of taps, separated 1.27 cm (0.5 inch) both in streamwise and cross-stream directions, were installed on the end walls, immediately upstream of the test section. Over the exit region of the test section was a series of taps on the endwall, separated by 1.27 cm (0.5 inch). These taps and a single tuft were used for monitoring the approach flow and stagnation points on the leading edge of the airfoils while the two bleeds shown in Fig. 1 were adjusted to insure that the approach flow was proper, i.e. the stagnation streamlines met the blade leading edges at the design stagnation lines. A trailing wall extended the suction surface. Constant-static-pressure regions were verified with the taps on the end walls both upstream and downstream of the channel. The static pressure data taken in these regions, together with the total pressure measured with a pitot tube in the core flow, were used to calculate the inlet and exit flow velocities.

The suction wall of the test section was a piece of high-grade, reinforced, FR-4 fiberglass cut to the turbine airfoil configuration. The concave wall of the test section was made of a lexan sheet and several strengthening ribs. Both simulate the turbine airfoil. There were no significant secondary flow effects, since the airfoil aspect ratio was 6.

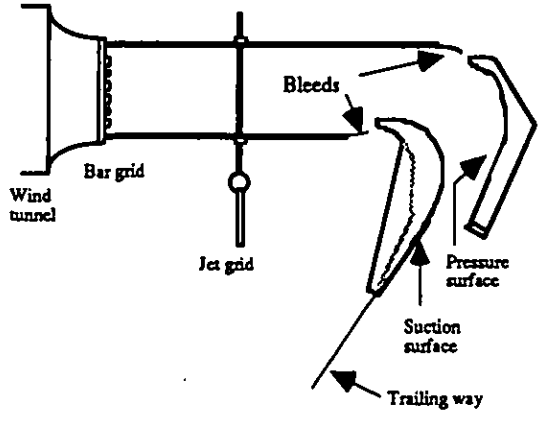

Fig. 1 Setup of the test section

In this study, a boundary layer type, single-wire, tungsten, hot-wire sensor of 4 μm diameter was placed in the flow over the convex wall for near-wall flow measurements. The probe y-direction movement was controlled by a stepper motor. With all near-wall velocity measurements, an intermittency analog circuit was utilized in combination with the hot-wire signal to evaluate the local flow state (laminar, turbulent, or transitional). A detailed description of the intermittency circuit design and its performance was given by Kim et al. (1994). A low-pressure transducer was used in conjunction with an impact tube to acquire total pressure and velocity data. The same transducer was connected to a set of 13 pressure taps on the suction wall for measurements of static pressure distributions. The coordinates of the pressure taps are listed in Table 1. A 12-bit, Norland Prowler digital oscilloscope was used for high-speed recording. Experiment control and data transfer were via an IEEE interface.

TABLE 1. Pressure tap locations on the suction surface

Tap #	x (cm)	x/L_X (%)	s (cm)	s/L_{SS} (%)
p1	0.00	0.00	0.00	0.00
p2	0.41	3.98	0.69	4.49
p3	2.17	21.11	2.72	17.78
p4	3.89	37.78	4.42	28.97
p5	4.80	46.67	5.34	34.96
p6	5.66	55.06	6.25	40.92
p7	6.43	62.47	7.17	46.96
p8	7.09	68.89	8.08	52.89
p9	7.67	74.57	9.00	58.95
p10	8.41	81.73	10.37	67.93
p11	8.84	85.93	11.28	73.84
p12	9.37	91.11	12.54	82.14
p13	10.01	97.28	14.14	92.61

QUALIFICATION AND UNCERTAINTY

The uniformities of free-stream velocity and turbulence of the approach flow were documented with a triple, hot-wire probe at several axial positions. For the low-FSTI cases, variations of average velocities and rms velocity fluctuations are less than 1% over the measured volume. The high FSTI cases had variations of velocities and fluctuations of 4 - 5%. Power spectra were taken one half chord length upstream of the inlet. Integral length scales are 4.85 cm and 4.2 cm for the 2.5% and 10% FSTI cases, respectively. Detailed documentation is presented in Qiu and Simon (1997)

Values of mean velocity were computed by summing over 4096 samples. The sample rate was set at 100 Hz for most of the measurements. The corresponding sample time was more than 40 seconds, which usually eliminated small-sample and low-frequency unsteadiness effects. The digitizer had sample-hold capabilities so values were "frozen" in less than a micro second. Since statistical values such as mean and turbulence intensity were sought, a sampling rate of 100 Hz was suitable. The uncertainty in both mean velocity and rms velocity fluctuation measurements is 3%, which is mainly caused by calibration error and misalignment. The instantaneous voltage output from the intermittency circuit is either zero, indicating laminar-like flow, or five volts, indicating turbulent-like flow. The time-average intermittency was evaluated by counting the number of five-volt points over 4096 samples. The intermittency circuit adjustments were made at the beginning of the test so that the intermittency function (which indicates the instantaneous state of the flow) agreed with the experimenter's interpretation of the state of the flow. This was done by viewing the hot-wire voltage waveform against the intermittency function waveform. To do this, both were digitized at 100 kHz to capture the waveform. This setting, once chosen, was used throughout the test program. The intermittency uncertainty is approximately 15 %. This was established by comparison of the hot-wire waveform and the intermittency function (details are in Kim et al. 1994).

MEASUREMENT

Static pressure distributions on the suction surface were measured with 13 surface pressure taps. The near-wall velocities were measured on the mid-plane of the test section. At each axial measurement station, the wall position was first located by viewing the probe, the wall, and the data as the probe was moved. The probe was then carefully brought to the wall and the traverse was initiated. A more detailed description of this wall-finding technique can be found in Qiu et al. (1995). Usually, velocity profiles were acquired with ~100 y-positions. This allowed sufficient spatial resolution to characterize the near-wall flow and identify the edge of the boundary or shear layer. More details of the facility and test section design, instrumentation (including intermittency measurement) and data processing are in Qiu and Simon (1997).

RESULTS AND DISCUSSIONS

Pressure profiles

Local static pressures, normalized as pressure coefficients, $C_p=2(p_t-p)/\rho U_e^2$, are compared to a fully-attached, high-Re number calculation (shown as the solid line) in Fig. 2. See Table 1 for pressure tap stations. The high-Re coefficient distribution was calculated by the manufacturer of the supplied airfoil shape. The same distribution was found with an invisid panel code and a Navier-Stokes code. At low FSTI (0.5%), two low-Reynolds-number flows (Re=50,000 and 100,000) start separation near station p8 (x/L_x=69%), as indicated by the end of a region of decreasing C_p (also supported by flow data to be discussed). The significant changes of Cp from p6 (x/L_x=55%) to p8 (x/L_x=69%) are due to a rapid growth of the unstable, laminar boundary layer flow. Two high-Reynolds-number flows (Re=200,000 and 300,000) do not separate until p9 (x/L_x=75%). The two low-Reynolds-number flows remain separated for the remainder of the suction surface length. For the Re=100,000 case, the separation bubble begins to shrink and the flow approaches reattachment near the trailing edge of the blade. In the Re=50,000 flow, there is no sign of reattachment. At Re=300,000, the flow is reattached to the wall near station p11 (x/L_x=86%) while the Re=200,000 flow remains separated until near p12 (x/L_x=91%). The 2.5% FSTI flows start with laminar boundary layer development through the accelerating flow section of the channel. Near the throat, low Reynolds number cases continue laminar boundary layer development until they reach a critical point where they separate, as with the low (0.5%) FSTI cases. High Reynolds number flows start transition of the attached boundary layer near the throat, preventing flow separation. Compared with low and moderate FSTI cases, high-FSTI (10%) cases have earlier transition. No separation was observed for the Re=200,000, 10% FSTI case.

Velocity profiles

Detailed velocity profiles, along with local turbulence intensities and intermittency distributions, were measured in the boundary layers for all Re and FSTI cases. Complete results were reported in Qiu and Simon (1997). In this paper, the Re=100,000, FSTI=2.5% case is chosen as the most representative case for the low-pressure turbine under the influence of a convected wake (Halstead et al. 1995). The chosen Re is near cruise conditions. The other cases with different FSTI and Re values are compared to this representative case and their effects are discussed.

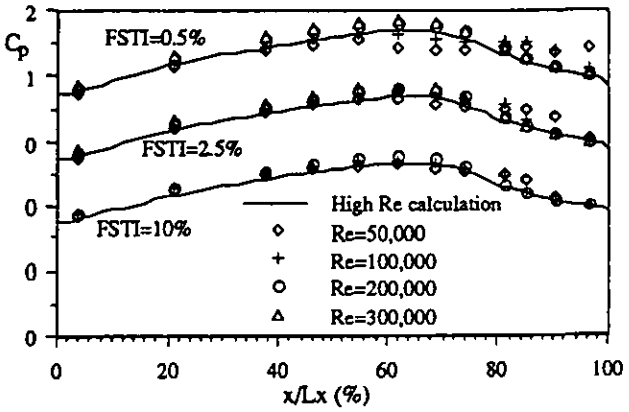

Fig. 2 Pressure distributions on suction surface

Velocity profiles measured from p8 (x/L_x=69%) to p13 (x/Lx=97%) are displayed in Fig. 3. Local turbulence intensities and intermittency distributions are shown in Figs. 4 and 5. At p8, the flow is a laminar, attached boundary layer (Fig. 3). Local turbulence intensities are less than 10% at this station (Fig. 4), so the mean velocity measurements are accurate throughout. Had the turbulence level risen to above 25%, the mean velocities taken with hot-wire anemometry would be artificially high for there would be times of reverse flow over the wire that would be interpreted by the wire as a forward flow. Flow has separated at p9 (x/Lx=74.6%). Separation is evidenced by near-zero velocities in the near-wall region (Fig. 3). The separation zone is about 0.6 mm thick. Measurements show zero intermittency at p8 and p9 over the full boundary layer thickness (Fig 5). Thus, transition has not begun and the flow is an attached, laminar boundary layer at p8 and a laminar, separated flow at p9. The separation bubble grows downstream in this decelerating flow region reaching 0.9 mm at p10 (x/Lx=81.7%).

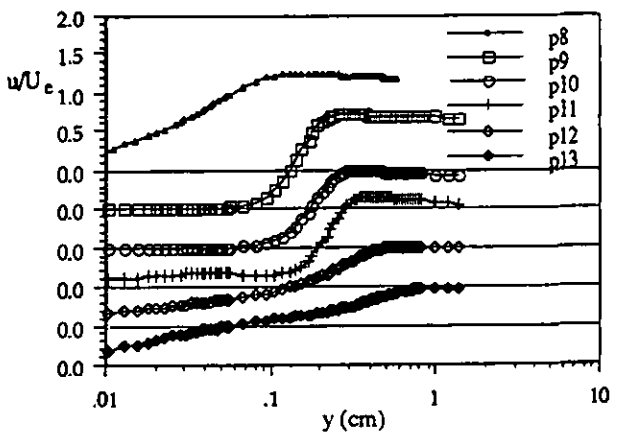

Fig. 3 Velocity profiles for the case of Re=100,000, FSTI=2.5% (see Table 1 for traverse locations)

The exceptionally high TI values at p10 (Fig. 4) are due to near-zero velocities of the fluid in the separation zone. The high turbulence intensities in most of the separated flow zones implies that the measured mean velocities are artificially high. Since these measured velocities are near zero, they are still accurate. The separation regions are essentially very dead zones with fluctuation amplitudes which are small, but large fractions of the mean velocities. This "dead zone" behavior was found also by Morin and Patrick (1991) The initiation of transition at p10 is evidenced by the intermittency profiles (Fig. 5). Detailed measurements show that this transition starts in the shear layer and propagates to the wall.

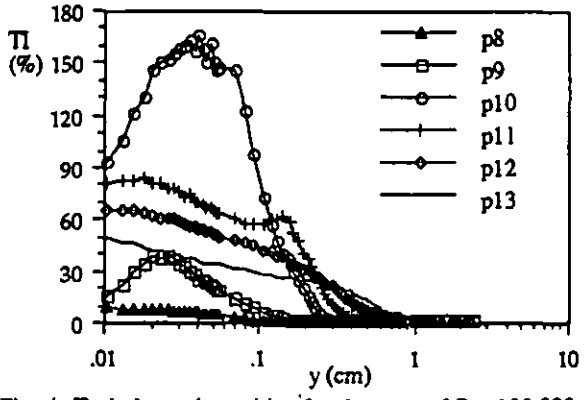

Fig. 4 Turbulence intensities for the case of Re=100,000, FSTI=2.5% (station locations are given in Table 1)

At p11 (x/Lx=85.9%), the separation zone has grown to 1.1 mm. This growth is attributed to a strong adverse pressure gradient. The shear layer has just transitioned at p10 and there is insufficient time for turbulent cross-stream transport of momentum to overcome the separation tendency. Local TI's at p11 are still high for this separated flow and the profile is beginning to assume a turbulent shape (Fig. 4). The turbulent state can also be seen in Fig. 5 where intermittency is over 0.8 from the shear layer to the separated, near-wall region.

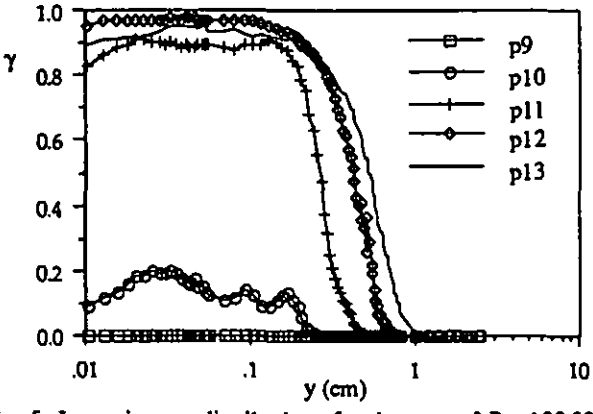

Fig. 5 Intermittency distributions for the case of Re=100,000, FSTI=2.5% (station locations are given in Table 1)

At p12 (x/Lx=91.1%), it appears that previously separated flow has reattached; turbulent transport has overcome the destabilizing effect of the adverse pressure gradient. The local TI is reduced for this newly reattached flow. Further downstream, p13 (x/Lx=97.3%), the flow is clearly reattached. The velocity profile is that of a turbulent boundary layer flow, though immature and different from that of a fully-developed turbulent boundary layer.

A sketch of the airfoil, with lines indicating the edge of the boundary layer and shear layer, for the case of Re=100,000 and FSTI=2.5% is given in Fig. 6. Boundary layer type (laminar or turbulent, attached or separated), onset of transition location, and separation point are marked in the sketch.

The Reynolds number effects on flow transition and separation can be seen in Figs. 7 and 8, velocity and intermittency profiles at p10 under FSTI=2.5% conditions. The separation bubble sizes for the Re=50,000, 100,000 and 200,000 case are 1.7 mm, 0.9 mm and 0.6 mm, respectively. The highest Reynolds number case (Re=300,000) is an attached turbulent boundary layer flow. The intermittency distribution, Fig. 8, shows that the Re=300,000 case has completed transition. Measurements show that for the Re=300,000 case transition started before p9 and this flow remained attached throughout the suction surface length. Station p9 is immediately after the throat and p10 is the strongest adverse pressure gradient location. The turbulent flow remained attached over the entire flow passage. Figure 8 shows that the Re=200,000 case is transitional, though near the end, while transition for the Re=100,000 case is in its early stages. No transition exists at p10 in the Re=50,000 case. Generally, the higher Re cases show earlier flow transition with enhanced turbulent transport and reduced possibility of flow separation or reduced separation zone sizes.

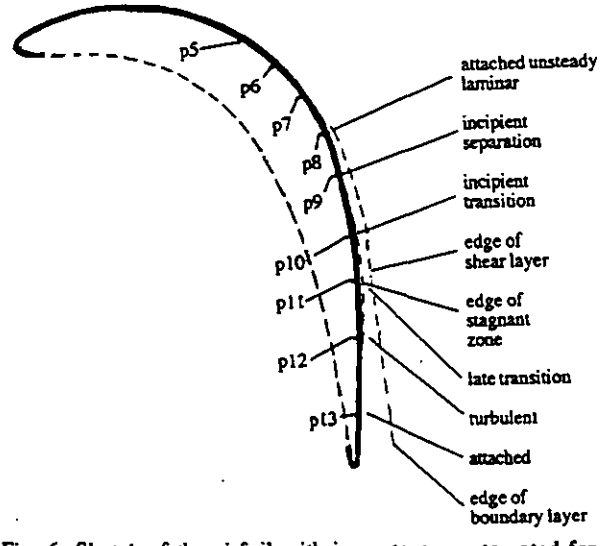

Fig. 6 Sketch of the airfoil with important events noted for the case of Re=100,000, FSTI=2.5% (station locations are given in Table 1)

High TI's for all four Re cases in Fig. 9 imply that measured velocities in the near-wall region are artificially high. Fluctuation profiles (u'/U_∞) are shown in Fig. 10. The Re=200,000 case has the highest fluctuation levels, since this flow is transitional, while the Re=300,000 flow has finished its transition process. Figure 10 shows that the Re=300,000 case has higher near-wall turbulence values whereas the other

cases that are beginning to transition in the separated shear layer show u'/U_∞ peaks in the center of the shear layer. Differences between turbulent and transitional boundary layer flows are noted in Fig. 10, where the u'/U_∞ profiles of the transitional flow (Re=100,000) have peak values in the shear layer while the u'/U_∞ profiles of the turbulent flow (Re=200,000 and 300,000) are more rounded and have their higher values at the wall.

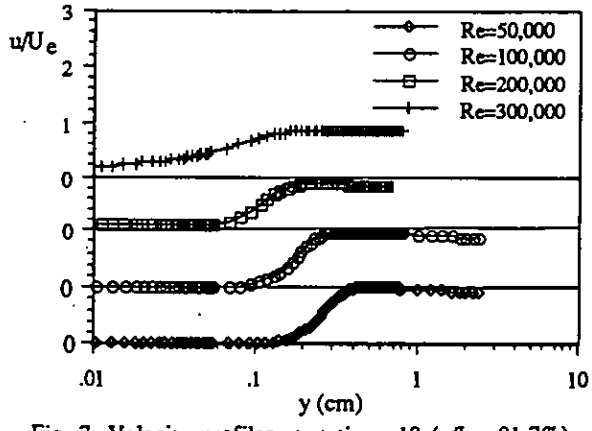

Fig. 7 Velocity profiles at station p10 (x/Lx=81.7%), FSTI=2.5%

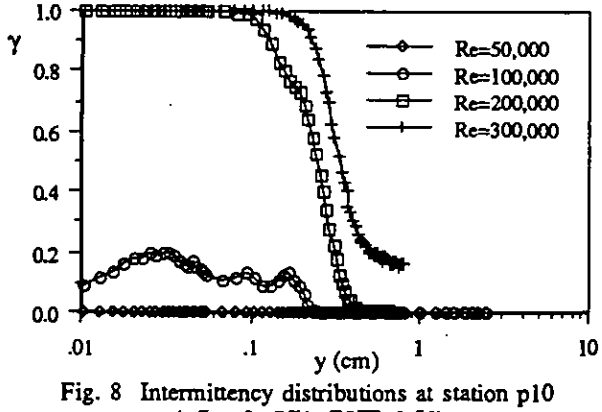

Fig. 8 Intermittency distributions at station p10 (x/Lx=81.7%), FSTI=2.5%

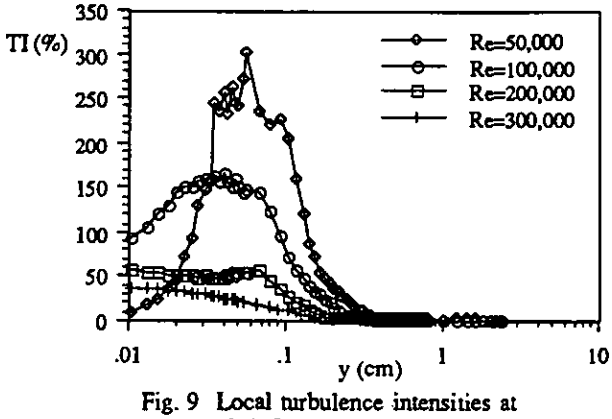

Fig. 9 Local turbulence intensities at station p10 (x/Lx=81.7%), FSTI=2.5%

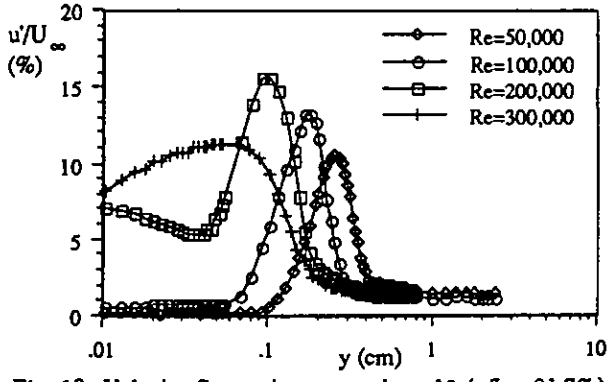

Fig. 10 Velocity fluctuations at station p10 (x/Lx=81.7%), FSTI=2.5%

The velocity profiles measured at p10 for the cases of Re=100,000 and FSTI=0.5%, 2.5%, and 10% are shown in Fig. 11. The intermittency profiles for these cases are plotted in Fig. 12. The effects of free stream turbulence intensity on flow transition and separation are clear. Figure 11 shows that the flows are separated for all three levels of FSTI but their separation bubble sizes are different. The FSTI=10% case has a separation bubble size of 0.8 mm while the separation zone is extended to 2.5 mm for the FSTI=0.5% case. Elevated FSTI induces earlier transition, as shown in Fig. 12. At p10, the flow of the FSTI=0.5% case is a separated laminar flow and no transition is indicated in the boundary layer. The FSTI=2.5% case has just started transition while the FSTI=10% case is within transition.

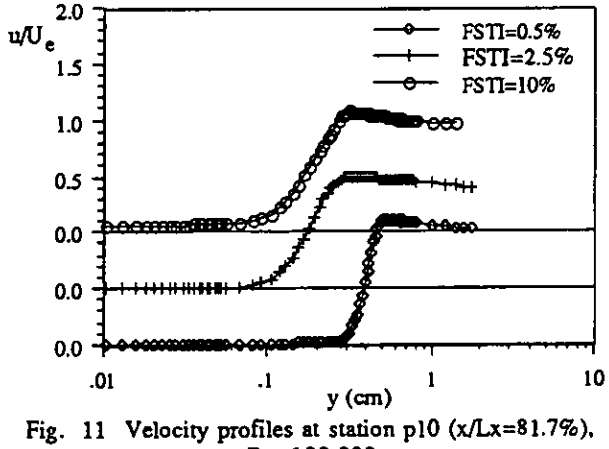

Fig. 11 Velocity profiles at station p10 (x/Lx=81.7%), Re=100,000

Separated Flow Transition Models

A model for intermittency during transition, computed from transition start and end locations, was developed by Narasimha (1984) from turbulent spot theory first suggested by Emmons (1951). A modified version of Narasimha's theory (Volino and Simon, 1995c) was applied to the present study. The peak (with y-direction) values of γ within the intermittency profiles were selected and used to calculate the function, $f(\gamma)=\sqrt{-\ln(1-\gamma)}$, which was then plotted versus streamwise location. Volino and Simon (1995c) found that in most flows

along flat-walls, the data lie along a straight line in these coordinates, although some exceptions may be seen at low γ (a phenomenon which Narasimha calls "pretransition"). A least-square fit to these data points can be extrapolated to $f(\gamma)=0$ and $f(\gamma)=2.146$, which correspond to $\gamma=0$ and $\gamma=0.99$, respectively. The corresponding axial positions, s, are taken as the locations of start and end of transition, s_{ts} and s_{te}. The transition start and end positions apparently depend on Re and FSTI, as discussed above. The intermittency within the transition region is plotted against the dimensionless streamwise coordinate $(s-s_{ts})/(s_{te}-s_{ts})$ in Fig. 13. Along with the measured data in Fig. 13 is the modified version (Volino and Simon, 1995c) of the Dhawan and Narasimha intermittency distribution model (1958). In the original Dhawan and Narasimha model, s_{ts} was taken at $\gamma=0.25$ and s_{te} was taken at $\gamma=0.75$. Here, s_{ts} is at $\gamma=0$ and s_{te} is taken at $\gamma=0.99$, following the recommendation of Volino and Simon (1995c). Agreement between the data and the model is good; especially considering that the model was developed for attached boundary layer flow transition whereas the data are for separated flow transition.

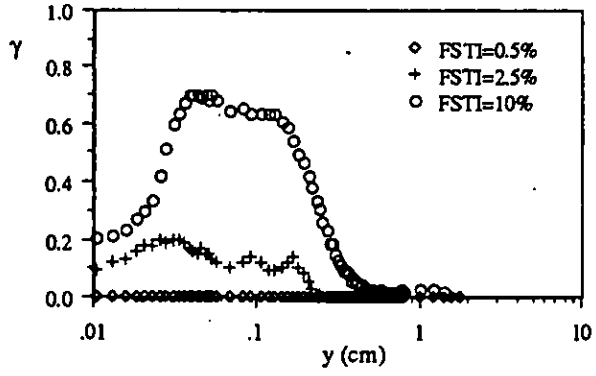

Fig. 12 Intermittency distributions at station p10 (x/Lx=81.7%), Re=100,000

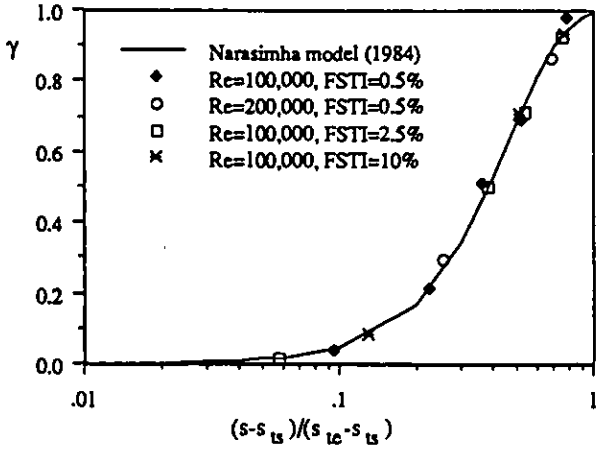

Fig. 13 Intermittency distributions through transition

The Reynolds numbers based on the distance between the separation point and the transition start point, $Re_{s_{st}}$, were computed from the measured data These Reynolds numbers are plotted in Fig. 14 as functions of $Re_{\delta 2_s}$, the Reynolds number based on momentum thickness at separation. Mayle's (1991) separated-flow models, Eqns. 1 and 2, are also shown in Fig. 14. Only low free-stream disturbance flows for Re less than 100,000 (FSTI=0.5%) agree with the long bubble model, as Mayle's model was developed from flows of FSTI=0.2-0.5% (Mayle 1991). Moderate and high free stream disturbance flows are distributed about the short bubble model line. In Fig. 15, transition length Reynolds number, Re_{LT}, is compared to Mayle's model, Eqn. 3. The model by Davis et al. (1985), Eqn. 4, represents an improvement (Fig. 16). This correlation seems to capture a turbulence intensity effect.

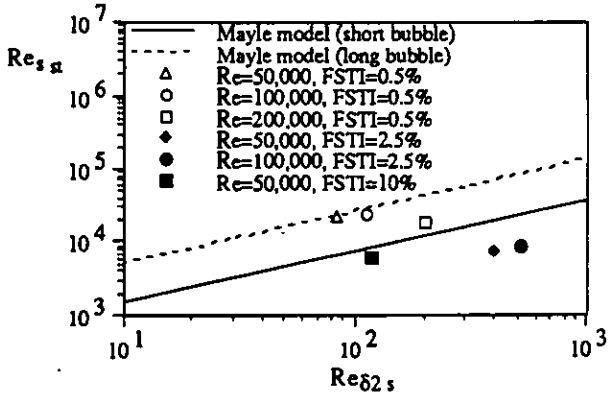

Fig. 14 Reynolds number based on distance between separation and transition versus separation Reynolds number

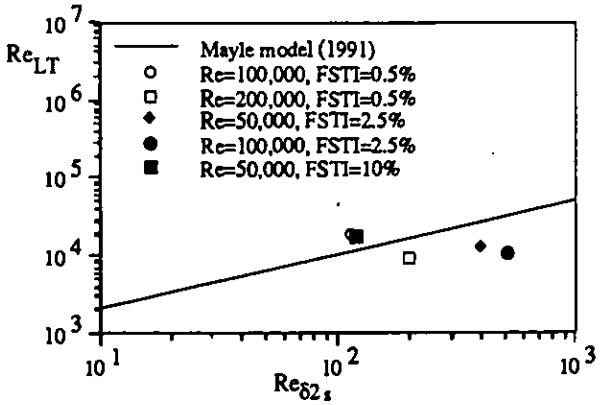

Fig. 15 Transition length Reynolds number in separation bubbles vs. separation momentum thickness Reynolds number

CONCLUSIONS

Velocity, pressure, and intermittency profiles were measured in boundary layers which simulate those on the suction surface of a low-pressure gas turbine airfoil. Detailed descriptions of cases with 2.5% FSTI and Re=100,000 are reported. Flow separation and transition in the separation region were observed for the cases of Re=50,000 and 100,000 with all free-

stream turbulence levels. No separation was found for the cases of Re=200,000 and FSTI=10% and Re=300,000, FSTI=2.5% due to early transition.

Transition in the shear layer over the separation bubble was found in all other separated flows, following the path: 1) laminar boundary layer development, 2) strong growth rate as a laminar boundary layer under adverse pressure gradient, 3) laminar separation, 4) transition of the free shear layer, 5) turbulent flow throughout the shear layer and near-wall region, 6) reattachment, and 7) growth as an attached turbulent boundary layer. The speed with which it proceeded through these steps and the degree to which it completed these steps increased as Re or FSTI increased.

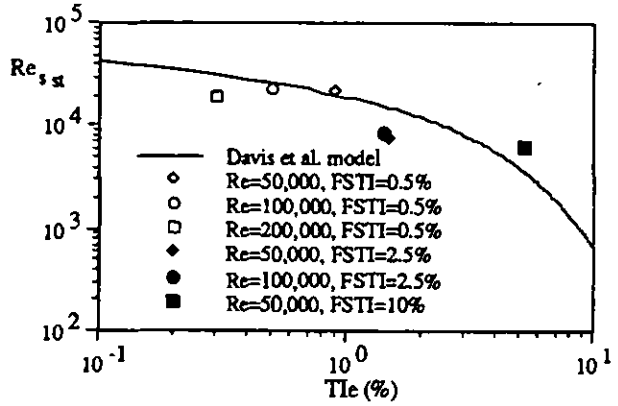

Fig. 16 Comparison of $Re_{s_{st}}$ to Davis et al. model (1985)

Table 2 summarizes all the cases investigated in this study. In the table, S indicates cases with separation, T denotes cases with transition.

TABLE 2 Conclusion of all the cases investigated

	Re=50K	Re=100K	Re=200K	Re=300K
FSTI=0.5%	S	S,T	S,T	S,T
FSTI=2.5%	S,T	S,T	S,T	T
FSTI=10%	S,T	S,T	T	(Not Done)

ACKNOWLEDGMENTS

This work was sponsored by NASA Lewis Research Center under grant NAG 3-1249. The contract monitor was Fred Simon.

REFERENCES

Davis, R. L., Cater, J. E. and Reshotko, E. (1985), "Analysis of Transitional Separation Bubbles on Infinite Swept Wings," AIAA Paper # AIAA-85-1685.

Dhawan, S. and Narasimha, R. (1958), "Some Properties of Boundary Layer Flow During the Transition of Inlet Turbulence and Rotor/Stator Interactions on the Aerodynamics and Heat Transfer of a Large-Scale Rotating Turbine Model," NASA CR 4079.

Emmons, H. W. (1951), "The Laminar-Turbulent Transition in a Boundary Layer - Part I," *J. Aero. Sci.*, Vol. 18, pp. 490-498.

Halstead, D. E., Wisler, D. C., Okiishi, T. H., Walker, G. J., Hodson, H. P. and Shin, H. (1995), "Boundary Layer Development in Axial Compressors and Turbines," ASME 4-part paper 95-GT-461 thru 464.

Kim, J., Simon, T. W. and Kestoras, M. (1994). "Fluid Mechanics and Heat Transfer Measurements in Transitional Boundary Layers Conditionally Sampled on Intermittency," *J. Turbo.*, Vol. 116, pp. 405-416.

Malkiel, E. and Mayle, R. J. (1995), "Transition in a Separation Bubble," ASME Paper 95-GT-32.

Mayle, R. E. (1991), "The Role of Laminar-Turbulent Transition in Gas Turbine Engines," *J Turbo.* , Vol. 113, pp. 509-537.

Morin, B. L. and Patrick, W. P. (1991), "Detailed Studies of a Large-Scale Laminar Separation Bubble on a Flat Plate," Vol. 1, UTRC Report No. R91-956786-1.

Narasimha, R. (1984), "On the Distribution of Intermittency in the Transition Region of a Boundary Layer," *J. Aero. Sci.*, Vol. 24, pp. 1-31.

Qiu, S. and Simon, T. W. (1997), "An Experimental Investigation of Laminar to Turbulent Flow Transition with Temporal and Spatial Acceleration Effects," NASA CR.

Qiu, S., Simon, T. W. and Volino R. J., (1995), "Evaluation of Local Wall Temperature, Heat Flux, and Convective Heat Transfer Coefficient From the Near-Wall Temperature Profile," Heat Transfer in Turbulent Flows, ASME HTD-Vol. 318, pp. 45-52.

Roberts, W. B. (1973), "A Study of the Effect of Reynolds Number and Laminar Separation Bubbles on the Flow through Compressor Cascades," D. Sc. Thesis, U. Libre de Bruxelles and VKI

Roberts, W. B. (1980), "calculation of Laminar Separation Bubbles and Their Effect on Airfoil Performance," *AIAA J.*, Vol. 18, No. 1, pp. 25-30.

Sahm, M. K. and Moffat, R. J. (1992), "Turbulent Boundary Layers with High Turbulence: Experimental Heat Transfer and Structure on Flat and Concave Walls," Internal Report, Dep. of Mech. Eng.., Stanford Univ., Stanford, CA.

Sharma, O. P., Ni, R. H. and Tanrikut, S. (1994), "Unsteady Flows in Turbines - Impact on Design Procedure," AGARD-LS-195, Paper No. 5.

Volino, R. J. and Simon, T. W. (1994), "Velocity and Temperature Profiles in Turbulent Boundary Layer Flows Experiencing Streamwise Pressure Gradients," ASME HTD-Vol. 285, pp. 17-24.

Volino, R. J. and T. W. Simon (1995a), "Bypass Transition in Boundary Layers Including Curvature and Favorable Pressure Gradient Effects," *J. Turbo.*, Vol. 117, pp. 166-174.

Volino, R. J. and Simon, T. W. (1995b), "Boundary Layer Transition Under High Free-Stream Turbulence And Strong Acceleration Conditions: Mean Flow Results," Proc. 4th ASME/JSME Thermal Engineering Joint Conference, Vol. 1, ed. L. S. Fletcher and T. Aihara, pp. 335-342.

Volino, R. J. and Simon, T. W. (1995c), "Measurements in Transitional Boundary Layers Under High Free-Stream Turbulence and Strong Acceleration Conditions," NASA CR-198413.